JOURNAL OF GEOPHYSICAL RESEARCH, VOL. 115, A07322, doi:10.1029/2009JA015170, 2010

On the generation of ELF/VLF waves for long-distance propagation via steerable HF heating of the lower ionosphere

M. B. Cohen,[1] U. S. Inan,[1,2] M. Gołkowski,[3] and N. G. Lehtinen[1]

Received 7 December 2009; revised 15 January 2010; accepted 8 March 2010; published 29 July 2010.

[1] ELF/VLF radio waves (300 Hz to 30 kHz) have been successfully generated via modulated HF (3–10 MHz) heating of the lower ionosphere in the presence of natural currents, most recently with the HAARP facility in Alaska. Generation is possible via amplitude modulation or via two techniques involving motion of the HF beam during the ELF/VLF cycle, known as beam painting and geometric modulation, described and measured by Cohen et al. (2010b). In this paper, we describe a theoretical model describing the HF heating and ionospheric responses, followed by a full-wave calculation of ELF/VLF propagation, and utilize this end-to-end model to derive the predicted radiated ELF/VLF pattern up to 1000 km from the HF heater in the Earth-ionosphere waveguide. We quantitatively compare the generated ELF/VLF signals on the ground from various generation techniques and find it to be generally in agreement with earlier measurements. We apply a simplified ELF/VLF propagation model to quantify the contribution of the ELF/VLF phased array in the radiation pattern resulting from geometric modulation and find this contribution to be significant. We also use a limited HF heating model to quantify the degree to which the current power level of HAARP is sufficient for the beam painting technique, since this technique requires high HF power densities at high altitudes.

Citation: Cohen, M. B., U. S. Inan, M. Gołkowski, and N. G. Lehtinen (2010), On the generation of ELF/VLF waves for long-distance propagation via steerable HF heating of the lower ionosphere, *J. Geophys. Res.*, *115*, A07322, doi:10.1029/2009JA015170.

1. Introduction

[2] ELF and VLF radio waves (300 Hz to 30 kHz) are fundamental to studies of the dynamics of the Earth's ionosphere and magnetosphere (see *Barr et al.* [2000] for a review). For instance, the ionospheric *D* region (i.e., below ~85 km) is not accessible by orbiting satellites, balloons, or (in many circumstances) high-frequency waves, making ELF/VLF radio remote sensing one of the only means for continuous measurement of lower ionospheric conditions. Moreover, ELF/VLF waves are unique due to their efficient global propagation (attenuation rates of only a few dB/Mm [*Davies*, 1990, pp. 389]) in the so-called Earth-ionosphere waveguide and relatively deep penetration into seawater (skin depths of tens of meters), which enables communications with submerged submarines, and global navigation. ELF/VLF waves have also emerged as a potentially useful tool for geophysical prospecting [*McNeil and Labson*, 1991].

[3] Unfortunately, generation of ELF/VLF waves poses an engineering challenge [*Watt*, 1967], since the wavelengths are many kilometers long, and the Earth's surface is a good conductor at these frequencies. ELF/VLF wave generation via high-frequency (HF) (3–10 MHz) heating of the ionosphere has the potential to overcome these difficulties and has been a subject of research since the first observations in Russia [*Getmantsev et al.*, 1974] and Norway [*Stubbe et al.*, 1981]. Utilizing the electron-temperature-dependent conductivity of the lower ionosphere, natural ionospheric currents such as the auroral electrojet can be modulated if the ionospheric electrons can be heated by more easily generated HF waves at ELF/VLF periodicities. Most ELF/VLF experiments utilizing HF heating have involved amplitude modulation, with the HF power simply ON-OFF modulated in time at the desired ELF/VLF frequency.

[4] More recently, the High Frequency Active Auroral Research Program (HAARP) phased-array high-frequency facility near Gakona, Alaska (62° 22′ N, 145° 9′ W), has been used to generate ELF signals that have been observed as far as 4400 km [*Moore et al.*, 2007; *Cohen et al.*, 2010a], as well as injected into the magnetosphere and observed in the geomagnetic conjugate region [*Gołkowski et al.*, 2008], although generation efficiencies remain quite low. In 2007, an upgrade of HAARP was completed, increasing its capacity from 48 active elements, 960 kW input power, and 175 MW effective radiated power (ERP), to 180 active elements, 3.6 MW input power, and ~575 MW ERP (at 3.25 MHz) [*Cohen et al.*, 2008a].

[1] STAR Laboratory, Stanford University, Stanford, California, USA.
[2] Department of Electrical Engineering, Koc University, Istanbul, Turkey.
[3] Department of Electrical Engineering, University of Colorado at Denver, Denver, Colorado, USA.

0148-0227/10/2009JA015170

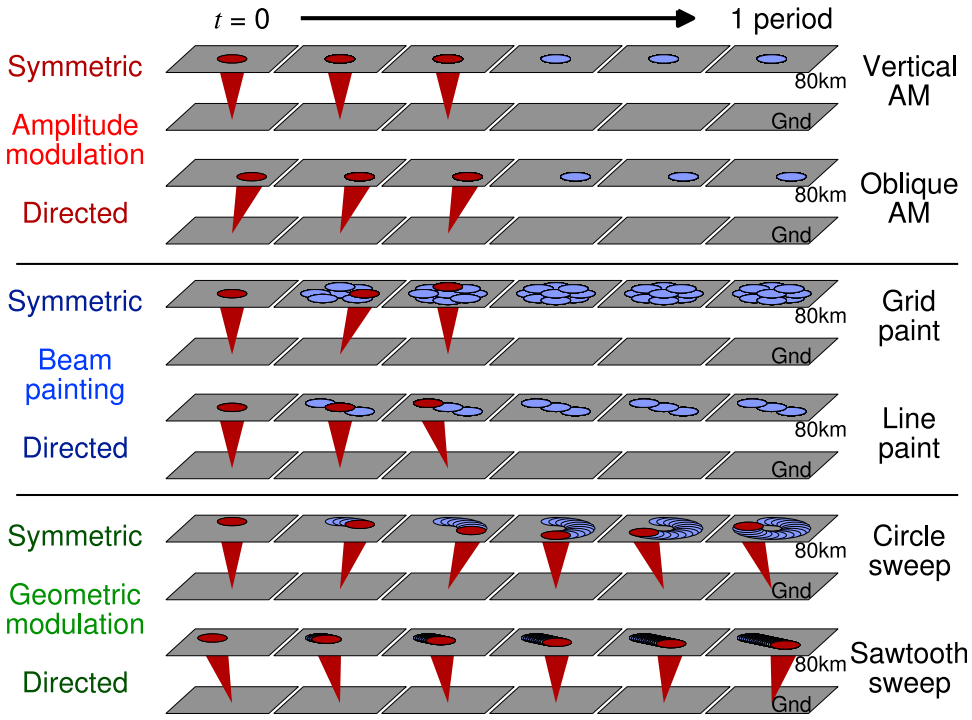

Figure 1. Schematic view of six forms of HF modulation, amplitude modulation, beam painting, and geometric modulation, each implemented in a symmetric or directed form. The directed forms are implemented oriented toward the bottom left.

[5] The HAARP array is capable of steering the HF beam over a cone 30° from vertical and can also provide rapid (up to 100 kHz) steering over a ±15° cone from a selected tune point. We discuss two techniques to utilize this HF beam motion to increase the ELF/VLF generated amplitudes and yield directional control of ELF/VLF power launched into the Earth-ionosphere waveguide.

[6] *Cohen et al.* [2008b] present first results from a technique therein referred to as "geometric modulation," which involves no HF power modulation but rather the movement of the HF beam in a geometric pattern with repetition rates at the desired ELF/VLF frequency. Geometric modulation is to some extent a more generalized extension of the two-element array experimentally discussed by *Barr et al.* [1987] and *Werner et al.* [1990] and the coherent sweep theoretically discussed by *Borisov et al.* [1996], with a small contribution from the oblique angle of the HF beam as discussed by *Barr et al.* [1988].

[7] The so-called "beam painting" technique proposed by *Papadopoulos et al.* [1989] involves rapidly scanning the HF heating beam over a large area during the ON portion of the ELF/VLF period, spending equal amounts of time between a series of beam locations but returning to each location before the electrons have had a chance to cool significantly. This technique enables a larger area of the ionosphere to be heated, implying a larger antenna and stronger ELF/VLF generation. *Cohen et al.* [2010b] experimentally compare beam painting with geometric modulation, as well as AM heating with an oblique HF beam. In this paper, we explore the comparison theoretically.

[8] Figure 1 shows the evolution of the HF beam direction over time for amplitude modulation, beam painting, and geometric modulation, each of which can be implemented in a symmetric form (where the beam motion does not favor a particular direction) or a directed form (where the beam motion favors a chosen azimuth). It should be noted that the beam painting involved very rapid (100 kHz) beam scanning, so the beam actually jumps locations several times between each cartoon but spends an equal time on each location as implemented here. We thus consider two types of amplitude modulation (vertical AM and oblique AM), two types of beam painting (line paint and grid paint), and two types of geometric modulation (circle sweep and sawtooth sweep), as shown in Figure 1. These terminologies are used herein to refer to the six types of beam motions. We consider beam tilting to be limited over a cone ±15° from vertical in any direction, in line with current HAARP capabilities.

2. Theoretical Model

[9] We utilize a theoretical model designed to reproduce the most important features of the HF-ELF/VLF conversion and propagation process. The approach to HF heating is similar to that used in past work [*Tomko*, 1981; *James*, 1985; *Rietveld et al.*, 1986; *Moore*, 2007; *Payne et al.*, 2007], in which the HF energy is propagated upward through the ionosphere, in vertical slabs. At each altitude, an energy balance equation is solved to keep track of the time-varying electron temperature dT_e/dt

$$\frac{3}{2}N_e k_B \frac{dT_e}{dt} = 2k\chi S - L_e(T_e - T_0) \quad (1)$$

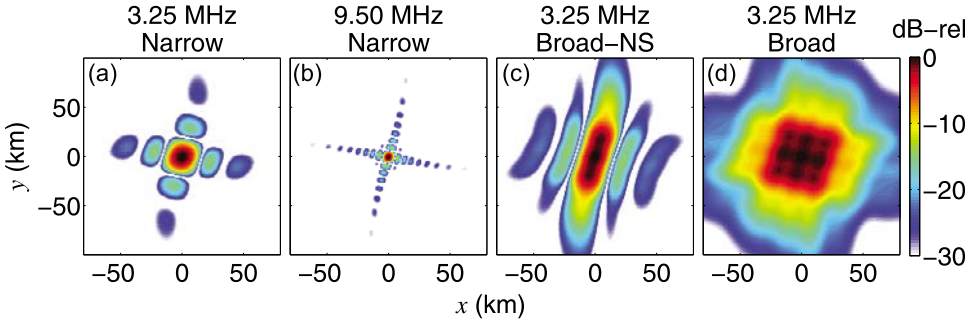

Figure 2. Relative power densities at 60 km from the HAARP HF array, in four beam modes, (a) 3.25 MHz "narrow beam," (b) 9.50 MHz "narrow beam," (c) 3.25 MHz broadened in the north-south direction, and (d) 3.25 MHz broadened in both directions.

where N_e is the electron density, k_B is Boltzmann's constant, k is the wave number, χ is the imaginary (absorbing) part of the refractive index calculated from the Appleton-Hartree equation, S is the HF power density, and L_e is a sum of electron loss terms, each a function of deviation from ambient electron temperature (T_0). We assume that the electron energy distribution remains Maxwellian through the heating and cooling process.

[10] A realistic HF radiation pattern from the HAARP array (including the sidelobes) is used to determine the spatial distribution of HF wave power at the base of the ionosphere. Figure 2 shows the relative HF energy entering the ionosphere (60 km altitude), for several different HAARP beam modes. The simulations shown here are carried out at an HF frequency of 3.25 MHz, with a "narrow" beam configuration, as shown in Figure 2a. The sidelobes of HAARP have ~15 dB lower power density in this mode but are taken into account in these simulations. HAARP can also operate at frequencies up to 9.5 MHz (Figure 2b), where the beam is thinner and more focused and the sidelobes are more numerous (but weaker). HAARP is also capable of broadening the beam either in one direction (Figure 2c) or in both directions (Figure 2d) in such a way as to merge the main beam with the sidelobes; thus spreading the power over a larger area via a technique discussed by *McCarrick et al.* [1990].

[11] We utilize a typical winter daytime high-latitude ionospheric profile derived from the International Reference Ionosphere and extrapolated at lower altitudes with an exponential profile [*Wait and Spies*, 1964]. We apply geomagnetic field values from the IGRF-10 model.

[12] At each altitude, HF energy absorption is calculated, and the remaining power is propagated upward. In the three-dimensional model discussed here, the bending and slowing of the HF energy as it propagates upward in an increasingly dense ionosphere is also taken into account. The electron temperature and collision frequency are calculated forward in discrete time steps, and the modified collision frequency is used as input in the next time step, so that the so-called "self-absorption" effects are intrinsically included. Several ELF/VLF cycles are calculated, until the electron temperature variations reach a periodic steady state. The ionospheric conductivity tensor is then calculated from the modified electron temperature. A short-time Fourier series is then applied to the last ELF/VLF period of the modulated ionospheric conductivity to extract the amplitude and phase of the periodic conductivity variation at the (fundamental) modulation frequency.

[13] We apply Ohm's law to convert the modulated conductivities to AC current sources in the ionosphere, assuming ambient electrojet electric field of 10 mV/m in the geomagnetic north direction. The resulting current sources in the ionosphere must be converted into magnetic fields after accounting for propagation in the ionospheric plasma medium. We thus apply a model of Earth-ionosphere wave propagation described in detail by *Lehtinen and Inan* [2008, 2009]. It takes advantage of Snell's law in the plane-stratified medium to calculate the electromagnetic field for each horizontal wave vector component $\mathbf{k}_\perp$ in the Fourier decomposition over horizontal coordinates $\mathbf{r}_\perp$. At each $\mathbf{k}_\perp$, the reflection coefficients and mode amplitudes are calculated recursively in a direction which provides stability against the numerical "swamping" which is inherent in many similar methods [*Budden*, 1985, pp. 574–576]. The configuration-space field is obtained by taking the inverse Fourier transform $\mathbf{k}_\perp \rightarrow \mathbf{r}_\perp$. The method can treat arbitrary harmonically varying sources by applying appropriate boundary conditions between the strata of the medium. The values of $\mathbf{k}_\perp$ for field calculations are taken at grid points on an optimized mesh.

[14] The propagation model (along with an earlier version of the HF heating model discussed by *Payne et al.* [2007]) has been previously utilized to characterize a "beam" of radiation emanating upward into the magnetosphere from the modulated HF heated region [*Lehtinen and Inan*, 2008], which was subsequently observed experimentally [*Piddyachiy et al.*, 2008]. Unlike the HF heating model, however, the ionosphere is assumed to be horizontally stratified and time-invariant so that the collision frequency modifications induced by the HF heating (and its subsequent impacts on ELF/VLF propagation) are ignored. *Lehtinen and Inan* [2008] estimate at worst 20–30% error due to this assumption in estimating radiated electromagnetic fields from modulated HF heating of the lower ionosphere. Earlier propagation models applied to modulated HF heating have instead focused on an analytical modal approach to ELF/VLF wave propagation [*Barr and Stubbe*, 1984; *Carroll and Ferraro*, 1990].

[15] Figure 3 shows the modeled magnetic fields on the ground resulting from a vertically directed HF beam at 3.25 MHz, amplitude modulated at 3 kHz. Figures 3a–3c show the x component of the magnetic field, while

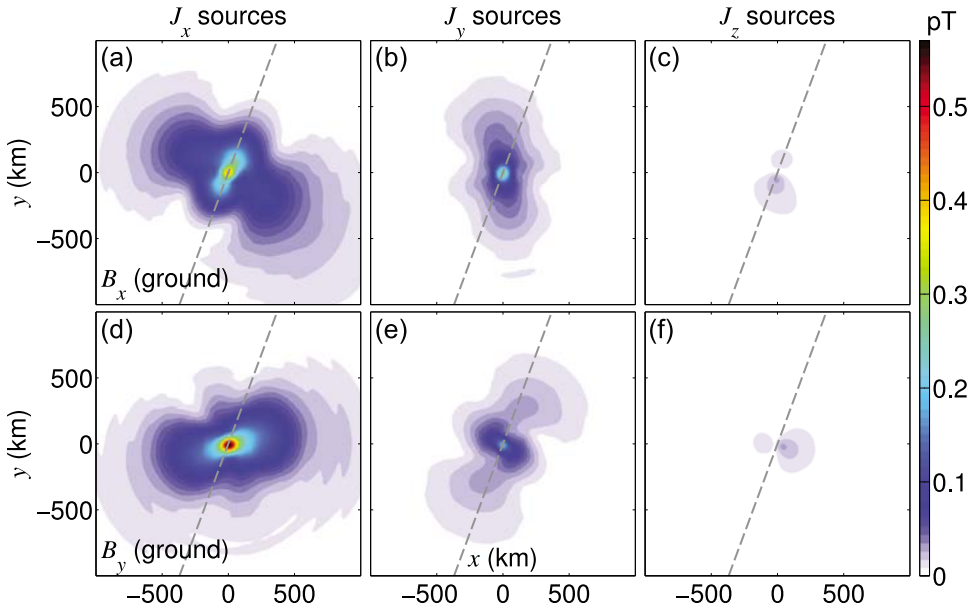

Figure 3. Propagation model results from HF heating simulation at 3 kHz, with vertical AM heating at 3.25 MHz. Horizontal magnetic fields on the ground over 1000 km area are shown, separately divided for sources in the (a and d) x direction, (b and e) y direction, and (c and f) z direction. Figures 3a–3c show the x component of received magnetic field, and Figures 3d–3f show the y component. The dashed line is the direction of geomagnetic north-south.

Figures 3d–3f show the y component. In this example, the model is separately run with only the x-directed current source components (Figures 3a and 3d), y-directed (Figures 3b and 3e), and z-directed (Figures 3c and 3f). The much smaller sources in the z direction arise only because of the 14° tilt of the geomagnetic field from vertical, and so the contribution to the magnetic field on the ground is small.

[16] If the current sources were radiating in free space, then x-directed current sources would produce only B_y fields on the ground, and y-directed current sources would produce only B_x fields on the ground, and the pattern on the ground would be symmetric about the x and y axis, respectively. This pattern can be roughly observed in Figures 3b and 3d. However, these sources are actually radiating in an anisotropic, lossy plasma and are therefore subject to mode conversion, so the x-directed current sources produce some B_x fields on the ground, and the y-directed current sources produce some B_y fields on the ground. Although weaker, these effects can be observed in Figures 3a and 3e, where it can also be seen that the pattern on the ground is roughly symmetric about the horizontal component of the geomagnetic field (shown by dashed lines).

[17] Thus by dividing up the radiating sources as such, we can observe that the pattern observed on the ground is essentially a sum of two components, one larger component from direct free-space propagation, and a second component resulting from mode conversion in the ionosphere

3. Generation Techniques

[18] We now quantitatively compare the ionospheric modulated currents from the various modulation techniques. Figure 4 shows a horizontal slice (at 75 km altitude) of the modulated Hall currents, with each of the six implementations from Figure 1 represented in a column, and six steps in the ELF/VLF cycle represented by the six rows. The simulations are for 3.25 MHz HF heating, at 5 kHz modulation frequency. The directed implementations (oblique AM, line paint, and sawtooth sweep) are modeled with the beam locations along azimuth 127° east of north (toward the southeast). The red color indicates positive currents (i.e., in the direction of the $\vec{E} \times \vec{B}_0$, where $\vec{E}$ is the auroral electrojet field), while the blue areas indicate negative. Since we plot here the Fourier-extracted first harmonic of the currents, all currents and fields simply vary sinusoidally with some amplitude and phase.

[19] Since the lower rows depict later points in time, the temporal behavior of the different modulation schemes is apparent in Figure 4. In the vertical AM, grid paint, oblique AM, and line paint columns, the currents in the center of the main beam reach a peak slightly earlier than the currents at outside edges of the main beam due to a longer propagation path for obliquely propagating HF energy, as discussed by *Barr et al.* [1988]. However, aside from this propagation effect, the currents are generally in phase since the heating and cooling begins and ends at the same time.

[20] The circle sweep and sawtooth sweep currents, in the third and sixth columns, appear to behave quite differently. Here, we have both positive and negative currents present at any given time. In fact, as time advances, the entire pattern of positive and negative currents moves. The circle sweep forms two swaths of currents, one positive and one negative, which rotate in a circular manner. The sawtooth sweep contains a few swaths, which travel along a line to the southeast direction. In other words, the two geometric modulation schemes appear to generate a moving source in the direction of the HF beam sweep.

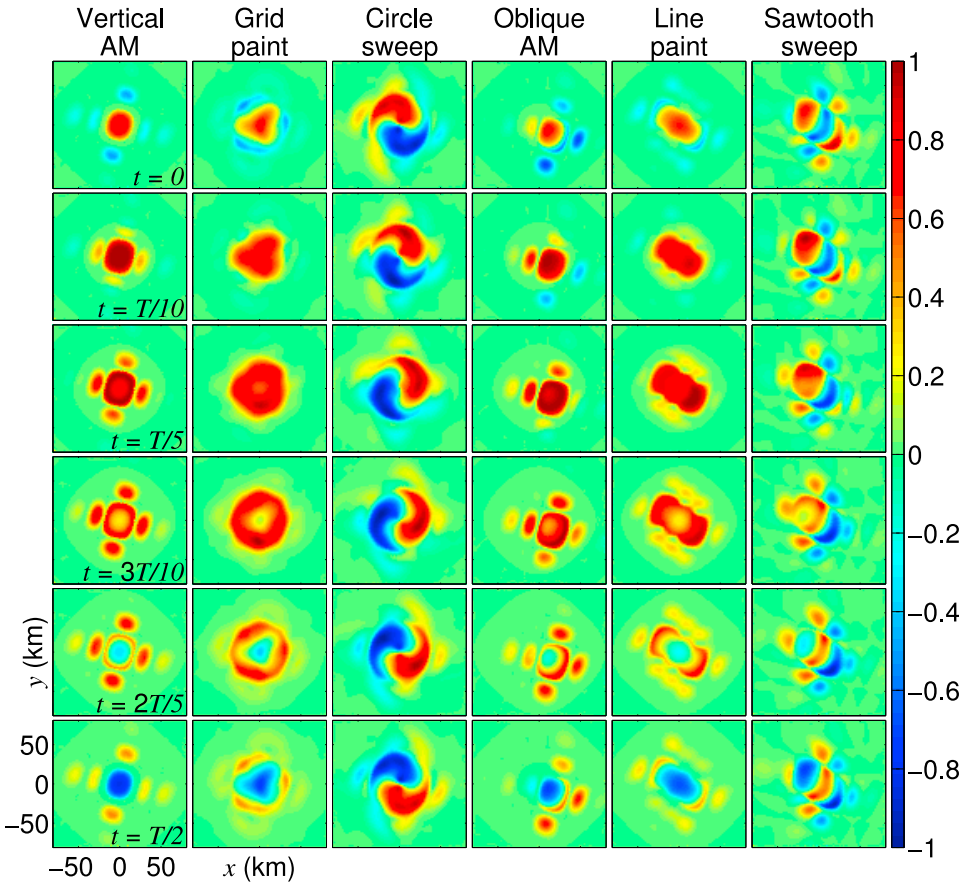

Figure 4. Results from the HF heating model applied to various modulation methods. Horizontal slices (at 75 km altitude) of the 5-kHz modulated Hall currents, after Fourier-extraction of the first harmonic. The columns show the six implementations from Figure 1, and the rows show six points during the ELF/VLF cycle.

[21] Figure 5 shows the result of the propagation model with these three dimensional currents from 5 kHz modulated HF heating at 3.25 MHz. The total horizontal magnetic field strength on the ground are shown over a 200 km × 200 km region centered at HAARP. Shown are the horizontal magnetic field on the ground from amplitude modulation (Figures 5a, 5d, and 5g), beam painting (Figures 5b, 5e, and 5h), and geometric modulation (Figure 5c, 5f, and 5i). The three rows show the symmetric implementation (Figures 5a–5c), directed implementation toward the southeast (Figures 5d–5f), and directed implementation toward southwest (Figures 5g–5i), as indicated by the arrows from the origin.

[22] The radiation pattern on the ground relatively near HAARP varies across the modulation techniques. For both amplitude modulation and beam painting, the strongest magnetic fields occur close to the HAARP facility, i.e., closest to the radiating ionospheric region. However, the oblique AM panels (directed amplitude modulation) appear to shift the center of the high-magnetic field patch away from the origin and toward the direction of the beam tilting.

[23] The magnetic fields near HAARP for the three beam painting techniques appear to be stronger than for the corresponding amplitude modulation techniques. However, apart from this patch of strong magnetic field near HAARP, the amplitude modulation and beam painting appear to be generally similar.

[24] In contrast, the character of the geometric modulation technique (as shown in Figures 5a, 5d, and 5g) appears quite different. In all three implementations, there is a local minimum underneath the heated ionosphere, due largely to an ELF/VLF phased array effect to be discussed later. For the circle sweep (or symmetric geometric modulation), this local minimum is a small circular patch, centered roughly at the origin, where the fields are a factor of ~5 lower than they are at ~60 km distance from the origin. For the sawtooth sweep (or directed geometric modulation), the local minimum is a swath passing through the origin, ~20 km thick, where the fields are ~5 times weaker than they are at ~60 km distance from the origin toward the sawtooth sweep azimuth.

[25] The nulls in the radiation pattern near the heated region are apparent for the geometric modulation schemes are in fact consistent with experimental observations noted by *Cohen et al.* [2008b] and *Cohen et al.* [2010b]. In particular, at a receiver near HAARP, the effectiveness of the geometric modulation circle sweep and sawtooth sweep appear to be similar to amplitude modulation, and less than that of beam painting, i.e., no enhancement in the ELF/VLF magnetic field is observed from geometric modulation at Chistochina. On the other hand, at Juneau and Kodiak, ~700 km away, the circle sweep, and sawtooth sweep

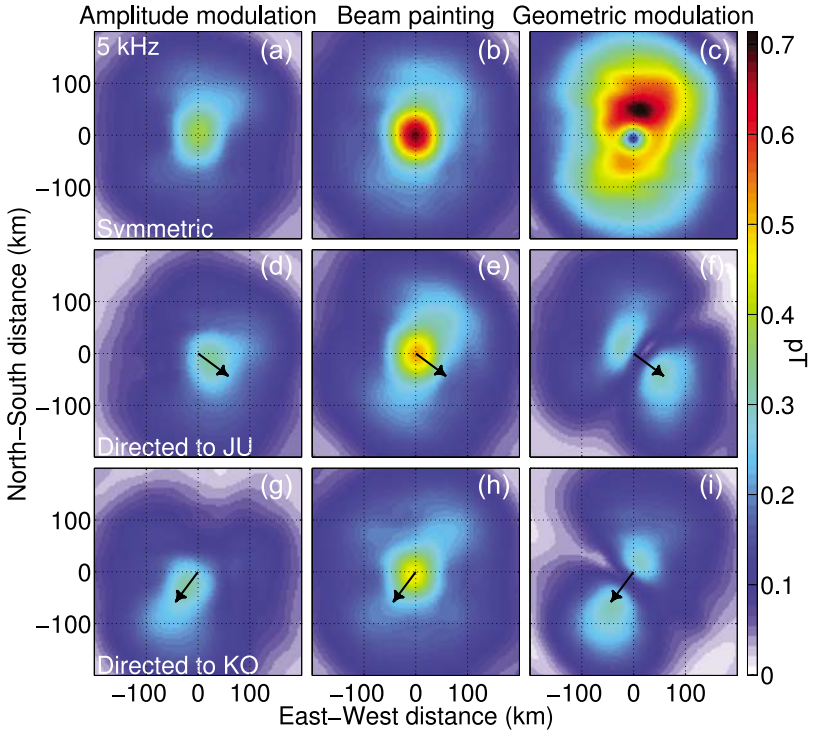

Figure 5. Modeled horizontal magnetic fields on the ground for (a, d, and g) amplitude modulation, (b, e, and h) beam painting, and (c, f, and i) geometric modulation. Each is simulated with a symmetric implementation (Figures 5a–5c), directed to JU and KO (Figures 5d–5i). Directions to JU and KO are indicated with arrows.

directed to the receiver generated substantially stronger signals.

[26] We now extend our view to longer distances. Figures 6–10 show the horizontal magnetic field on the ground up to a distance of 1000 km away from HAARP, at nine different frequencies from 1 to 9 kHz, for heating by oblique AM, grid paint, line paint, circle sweep, and sawtooth sweep, respectively. The directed formats are implemented toward the JU location shown on the grid, for comparison with measurements made earlier [*Cohen et al.*, 2010b]. Each grid point in the horizontal plane is normalized to the magnetic field amplitude for vertical AM, which serves here as a baseline for comparison since the bulk of ELF/VLF wave generation experiments with HF heating have utilized it.

[27] The red and yellow areas indicate stronger signals compared to vertical AM, and blue areas indicate weaker magnetic field signals compared to vertical AM. All of the plots exhibit a series of concentric circles of peaks and nulls. These circles result from the interference pattern of the multimode ELF/VLF waves propagating away from the source, especially at the higher frequencies (which is significantly above the Earth-ionosphere first order mode cutoff frequency of ~1.8 kHz), which is shifted as the ionospheric source size and orientation changes. The nulls and valleys also become closer as the wavelength becomes shorter. Experimental measurement of the comparative effectiveness between these modulation techniques may therefore be sensitive in part to the exact receiver location, with a few dB of magnetic field amplitude variation.

[28] The following frequency-dependent characteristics are present in the predicted magnetic field ratio plots:

[29] 1. The characteristics of oblique AM HF heating are presented in Figure 6. Below 3 kHz, oblique AM yields nearly identical magnetic fields compared to vertical AM. At increasing frequencies beyond 3 kHz, oblique AM begins to show a distinct radiation pattern in which the half-space in the direction of the beam tilt exhibits increased amplitudes (by ~5 dB by 8 kHz), whereas a corresponding decrease (of ~5 dB by 8 kHz) is seen in the half space in the other direction. The frequency dependence of the directionality likely arises from the finite size of the HF heated region, which becomes increasingly comparable to a wavelength with increasing frequency, as discussed by *Barr et al.* [1988].

[30] 2. The predicted radiation characteristics of grid paint HF heating are shown in Figure 7. Below ~3 kHz, the grid paint technique produces ~4 dB of amplitude gain, nearly uniformly by direction. With increasing ELF frequency, however, this advantage begins to disappear, and by 4 kHz, the overall ELF radiation is weaker than vertical AM in just as many areas as it is stronger. In other words, with increasing frequency, the improvement achieved with the grid paint appears to disappear. This feature likely arises from the large size of the heated region, which becomes an inefficient antenna when the size approaches that of a wavelength, due to destructive interference of the signal from different parts of the heated region. Since the heated region is much larger than in the case of AM heating, this frequency-dependent effect occurs at a lower frequency.

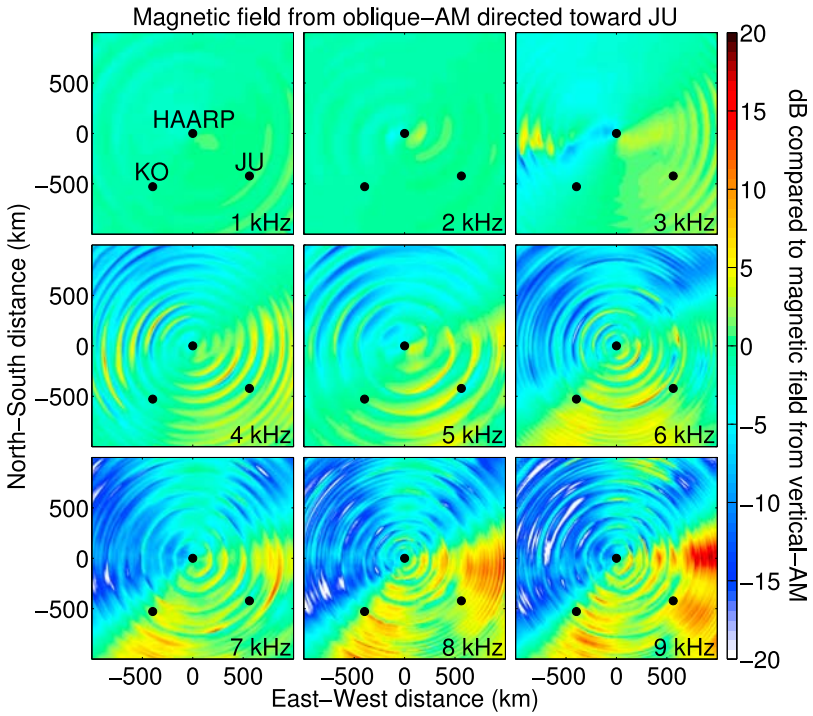

Figure 6. Modeled horizontal magnetic fields on the ground for oblique AM heating directed to JU, at nine different frequencies. The corresponding location of HAARP, and two receivers utilized extensively in past experiments (Juneau, JU, and Kodiak, KO), are shown with black dots.

[31] 3. The modeled ELF amplitudes from the line paint HF heating are demonstrated by Figure 8. The characteristics are, in fact, quite similar to those of the grid paint, with a nearly uniform amplitude gain (in this case, a few dB) at the lowest frequencies, which disappears as the frequency is increased to ~4 kHz. However, the line paint does appear to generate a clear directionality not apparent in the grid paint. For instance, at 4 kHz, radiation is preferentially launched in

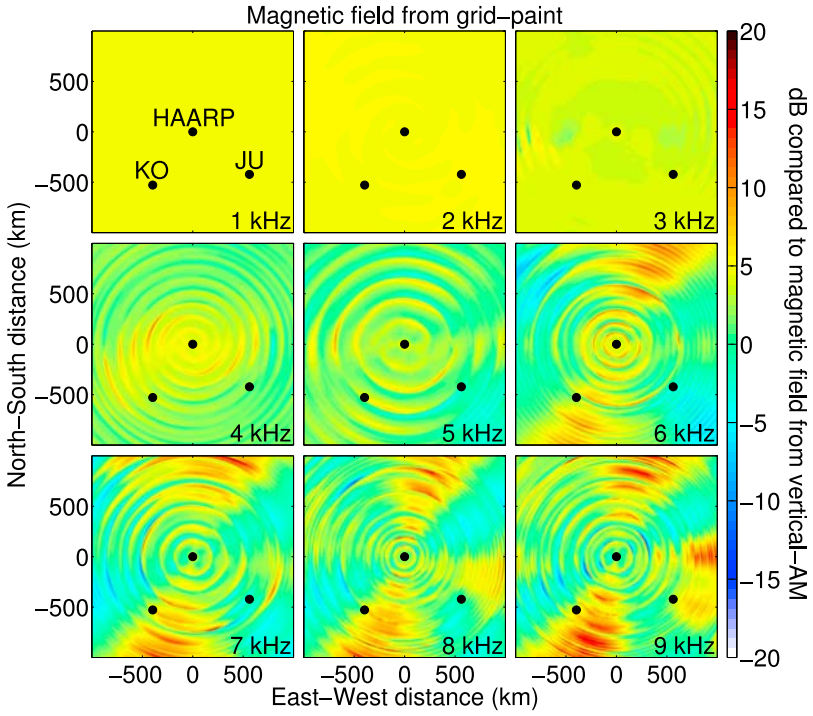

Figure 7. Same as Figure 6 but for the grid paint.

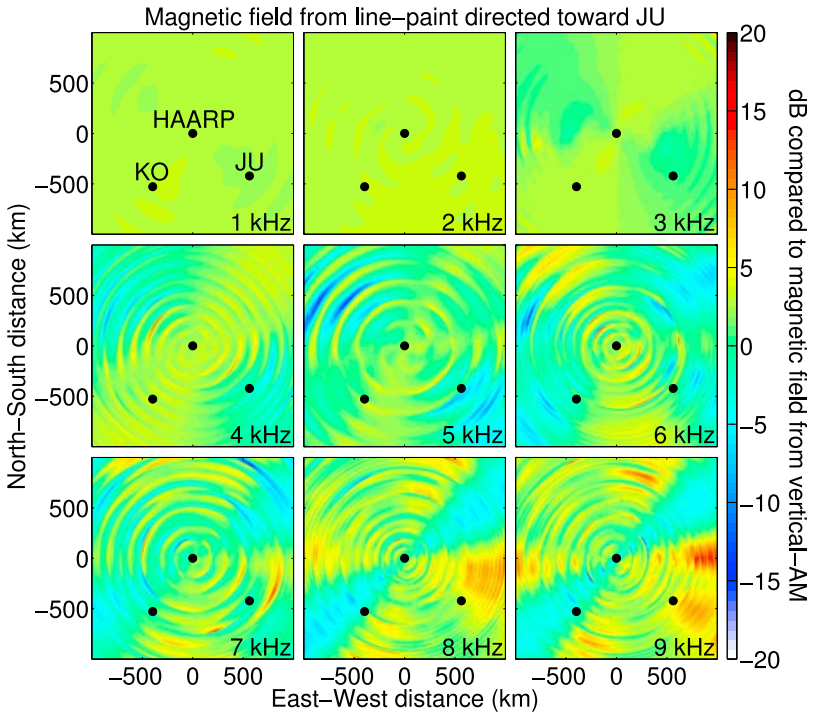

Figure 8. Same as Figure 6 but for the line paint directed to JU (i.e., the three cyclical HF beam locations are aligned along an azimuth to JU).

the direction orthogonal to the line paint orientation, as the heated region is elongated in the direction of JU, and therefore likely similar to a shortwave dipole. On the other hand, at frequencies closer to 8 kHz, the radiation is preferentially launched in the direction parallel to the line paint orientation, since at these frequencies, the heated region is more akin to a half-wave dipole.

[32] 4. The simulated characteristics of circle sweep HF heating can be seen in Figure 9. At 1 and 2 kHz, the circle sweep produces roughly the same magnetic field amplitudes

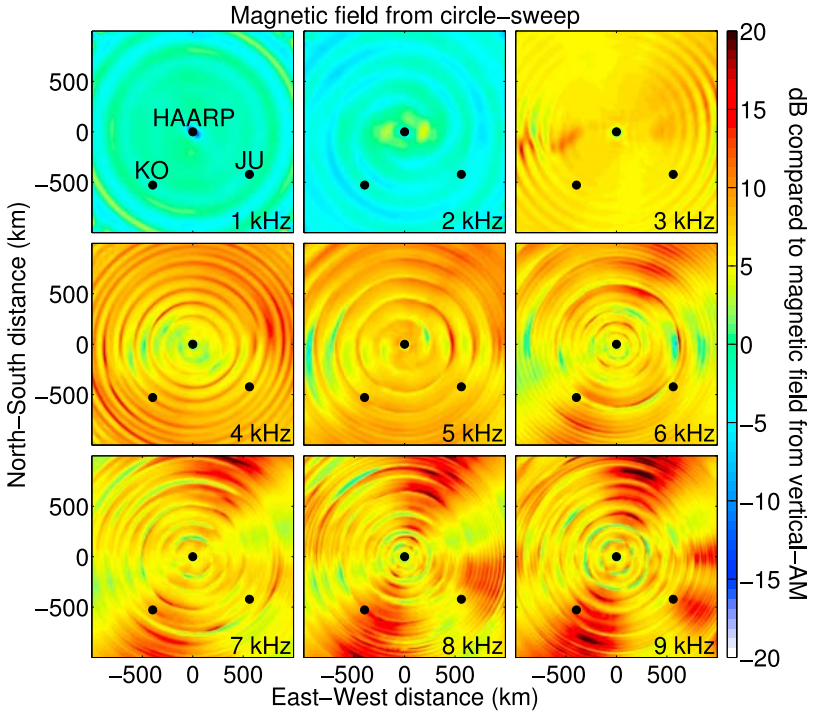

Figure 9. Same as Figure 6 but for the circle sweep.

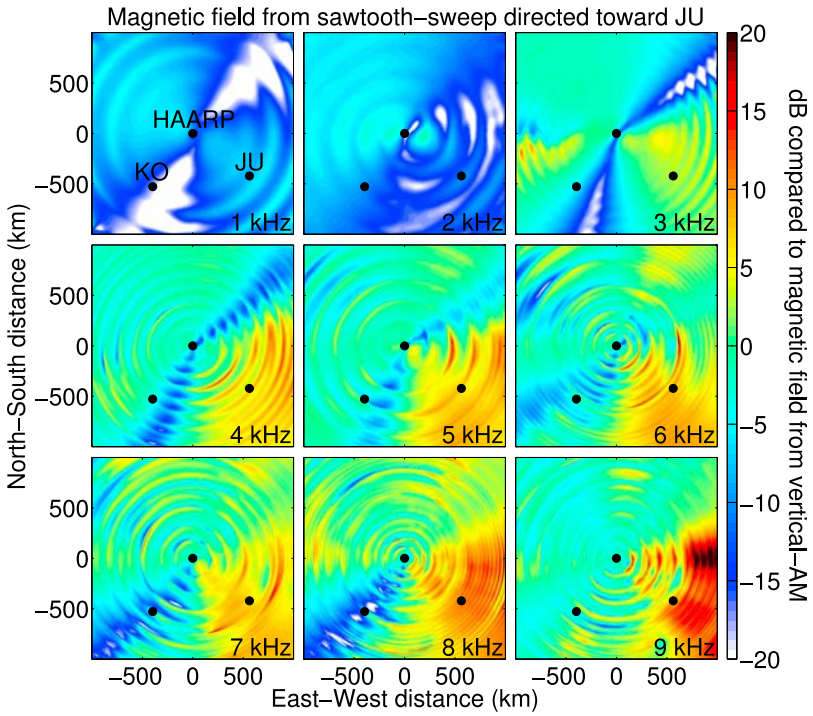

Figure 10. Same as Figure 6 but for the sawtooth sweep directed to JU (i.e., the HF beam repetitively sweeps in the direction of JU).

as vertical AM, but starting at 3 kHz, begins to demonstrate increasingly strong magnetic fields, by ~10 dB. The amplitude gains are essentially azimuthally uniform, although at the highest frequencies, some directionality appears in the north-northeast and south-southwest direction, which may be due to the presence of the small HF sidelobes of HAARP, which are oriented roughly in that direction. We are discussing the generated amplitudes, and it should be noted that the circle sweep (and sawtooth sweep) utilize 3 dB more HF power than amplitude modulation, so the higher amplitudes do not correspond directly to an efficiency measure.

[33] 5. The characteristics of sawtooth sweep heating can be observed in Figure 10. Below 3 kHz, the sawtooth sweep produces weaker signals compared to vertical AM, but beginning at frequencies at or above 3 kHz, the sawtooth sweep generates radiation preferentially in the direction of the sweep (toward JU), whose relative amplitude compared to vertical AM increases as a function of frequency, to as high as 15–20 dB by 9 kHz, i.e., much stronger than the directionality apparent from oblique AM. The preferential radiation is confined within a cone ~60–100° wide, depending on ELF frequency. In addition, while utilizing oblique AM increases the magnetic field in one half plane and decreases it correspondingly in the other, the sawtooth sweep seems to maintain the same magnetic field amplitudes outside of the cone. It can also be seen that the cone of enhanced radiation splits into two portions at 9 kHz. This effect may occur in part because the HF beam location at 75 km altitude moves laterally faster than the speed of light, so that the phase matching achieved via the beam motion is most effective at azimuths slightly off-center from the direction of the sawtooth sweep. Further study on the directional pattern may be required.

4. Comparison to Experiment

[34] We now compare these theoretical predictions to earlier measurements. *Cohen et al.* [2008b] and *Cohen et al.* [2010b] present comparative measurements of the magnetic field near to HAARP (37 km distance), and at two receivers at ~700 km distance and nearly orthogonal directions. At farther distances, geometric modulation is found to generate 7–11 dB stronger signals than vertical AM heating at farther distances (via the circle sweep), and provide 11–15 dB of directional control (depending on the azimuth of the sawtooth sweep), with ELF/VLF amplitudes higher in the direction of the sawtooth sweep azimuth. Beam painting is found to generate a small (2–4 dB) amplitude enhancement detectable only near to HAARP, and provides 4–6 dB directional control, with ELF/VLF amplitudes maximized in the direction orthogonal to the line paint.

[35] A complete set of measurements of the various techniques shown in Figure 1 is given in Figure 4 of *Cohen et al.* [2010b]. The three receivers utilized therein are in Chistochina (62.62°N, −144.62°W, 37 km from HAARP), Juneau (58.59°N, 134.90°W, 704 km from HAARP), and Kodiak (57.87°N, 152.88°W, 661 km from HAARP). Chistochina is located near to the HAARP facility, while Juneau and Kodiak are located in roughly orthogonal directions from HAARP, but at similar distances.

[36] We therefore extract the magnetic field at the locations in the simulation grid corresponding to the above receivers, and indicated with black dots in Figures 6–10.

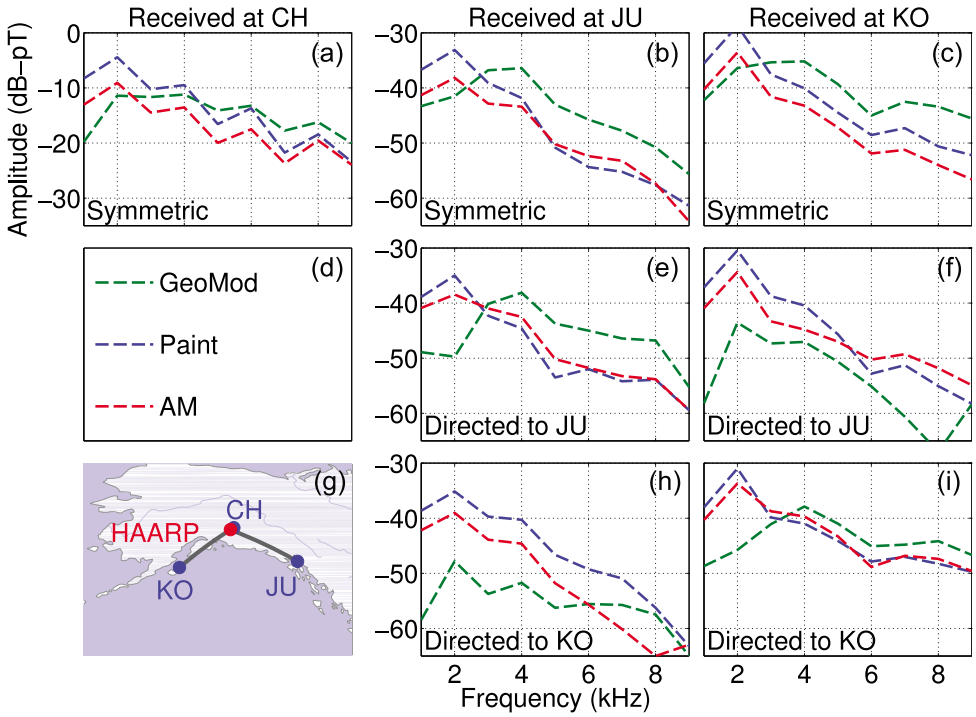

Figure 11. Simulation are repeated for a variety of frequencies between 1 and 9 kHz, and plotted together for direct comparison with Figure 4 of *Cohen et al.* [2010b]. Plotted are geometric modulation (green traces), beam painting (blue traces), and amplitude modulation (red traces), received at (a, d, and g) CH, (b, e, and h) JU, and (c, f, and i) KO, for symmetric implementation (Figures 11a–11c), directed to JU implementation (Figures 11d–11f), and directed to KO implementation (Figures 11g–11i).

Though not shown, the simulations are also repeated for oblique AM, line paint, and sawtooth sweeps directed to Kodiak. These magnetic field values are shown in Figure 11 for the purpose of direct comparison with Figure 4 of *Cohen et al.* [2010b]. The main features of the theoretical results match reasonably well the experimental measurements.

5. Point-Source Free Space Model

[37] We now discuss the notion of ELF/VLF phased array control, an aspect specific to geometric modulation. *Barr et al.* [1987] describe the creation of a two-element phased array, as a result of alternating the beam position between two locations in the ionosphere. Although only two independent spots (180° out of phase) were possible with the Tromsø facility, the distance between the two spots could be controlled.

[38] A significant extension of this concept is achieved via geometric modulation. There can be dozens of beam locations within the ELF/VLF cycle, each of which create separate and independent radiating regions, whose phases can be controlled by the order in which those regions are heated. If the beam locations in the circle sweep are thought of as forming a set of point sources, then those point sources radiate with phases varying around the circle and distributed equally.

[39] *Moore and Rietveld* [2009] and *Cohen et al.* [2009] discuss the role of the oblique angle of the HF beam as opposed to this phased array nature, with *Moore and Rietveld* [2009] proposing that the oblique angle may play a dominant role in the observations of *Cohen et al.* [2008b], while *Cohen et al.* [2009] argue that the phased-array nature is likely more significant. *Cohen et al.* [2010b] present additional experimental evidence on the impact of the oblique angle but cannot singularly isolate the effect of the phased array, since the HAARP HF beam cannot be made infinitely thin.

[40] In this paper we quantify the importance of this ELF/VLF phased array using a simplified model. A free-space model is applied, similar to that used in *Payne* [2007], in which a number of phased point sources are on a plane in free space, and the magnetic field at a parallel plane is subsequently calculated from the retarded magnetic vector potential. This approach intrinsically models only the geometric effects of the ELF/VLF phased array aspect. Figure 12 shows the horizontal magnetic field pattern on the ground (normalized) from the simplified free space model, within 200 km of HAARP, for both the circle sweep (Figure 12a) and sawtooth sweep (Figure 12b). There are 20 ideal 5 kHz sources placed in the ionosphere, at an altitude of 75 km and where the HF beam center is located. The sawtooth sweep is oriented toward Juneau, roughly to the southeast from HAARP.

[41] A number of important aspects are common to both Figures 12 and the corresponding plots in Figure 5c and 5f. For the circle sweep, there is a clear null in the center, a few tens of kilometers wide, directly underneath the center of the circle sweep. The sawtooth sweep features two regions/lobes of radiation on the ground, one larger lobe directed toward Juneau, and another smaller lobe immediately in the

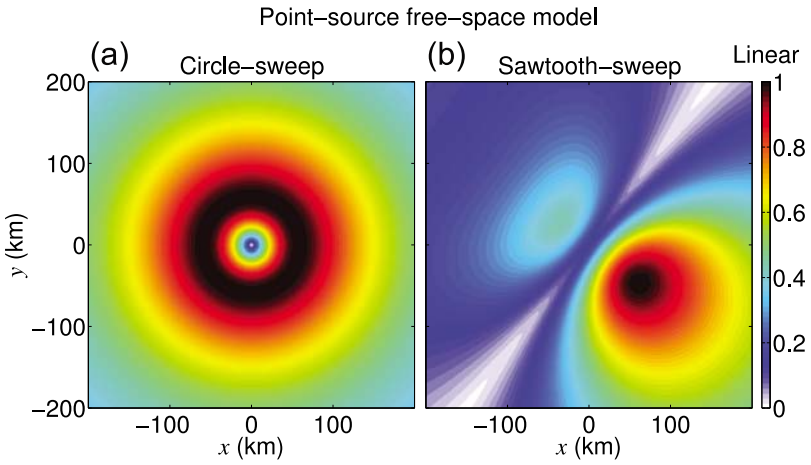

Figure 12. Point source free space model of fields on the ground for the (a) circle sweep and (b) sawtooth sweep to Juneau.

opposite direction. In between the two lobes is a null, extending from northeast to southwest, orthogonal to the direction of the sawtooth sweep. The full-model equivalents to the Figures 12a and 12b are in Figures 5c and 5f, respectively, and the similarity of these characteristics is an indication that the ELF/VLF phased array behavior plays a dominant role in determining the magnetic field structure on the ground.

[42] There are nonetheless some differences between the results from the point source model and the full theoretical model. In the full theoretical model, the null in the center is not surrounded by a symmetric "donut," as it is in the free-space model result. Since the sources in real life are embedded in a plasma rather than free space, this asymmetry may result from the 16° off-vertical tilt of the Earth's magnetic field. The peak of the magnetic field around the "donut" in Figure 12 occurs almost precisely in the geomagnetic northward direction from HAARP. In addition, for the case of the sawtooth sweep, the smaller lobe toward the northwest is much smaller than the main lobe for the point source model, whereas for the full theoretical model, there are about equal magnetic field values in each.

6. HF Pulsing in Beam Painting

[43] We now explore an important physical aspect that relates exclusively to beam painting. The technique of beam painting requires rapid motion of the HF beam to maintain a larger heated region of the ionosphere. A larger antenna gives the potential for more radiation. There is a tradeoff, however, because if the HF beam must scan between N locations, then during the ON portion of the ELF/VLF cycle, each point in the ionosphere is not heated continuously but is instead heated in short pulses (with HAARP being capable of pulses as short as 10 μs), with OFF times between the pulses, so that the heating is achieved with pulsed duty cycle HF radiation. Effective beam painting as originally proposed by *Papadopoulos et al.* [1989, 1990] therefore requires a very high power density in the HF beam, which implies a heating time constant much shorter than the cooling time constant, so that in the time between the pulses (when the beam is directed elsewhere) the electrons do not cool significantly. The required power levels and the resulting dynamics have been previously discussed [*Papadopoulos et al.*, 1989, 1990], so our purpose here is to apply these requirements to the case of HAARP, and quantify the loss of efficiency due to the finite ERP of the HAARP HF beam in the context of the model described earlier.

[44] Figure 13 shows schematically how an increasingly rapid heating rate enables the short pulses to sustain ionospheric conductivity. The black traces show the ON-OFF power density at a given ionospheric location. In this case, we show three 10 μs long pulses, separated by 20 μs, corresponding quite closely to the line paint, since the HF beam scans between three ionospheric locations. The green curve shows an exponential curve which approaches either 0 or 1, depending on the HF power. The heating and cooling occurs exponentially, with characteristic times τ_{heat} and τ_{cool}, respectively. This curve is a first-order approximation of the heating and cooling dynamics but one that has been employed previously [*Barr et al.*, 1999]. For $\tau_{cool} = 165\mu$s, as in the estimate given by *Barr et al.* [1999] for the modulation frequency and a daytime ionosphere.

[45] Figure 13a shows the case where the heating and cooling time constants are equal, Figure 13b shows the case for τ_{heat} ten times shorter than τ_{cool}, and Figure 13c shows the case τ_{heat} is 100 times shorter than τ_{cool}. As the heating time constant decreases, the average value of the conductivity change (shown with the dashed gray line) rises closer to 100%, despite the fact that the HF is ON for only one third of the time. For Figures 13a–13c, the fractional loss (i.e., the amount the gray line drops below 100%) corresponds to an amount of conductivity modulation lost as a result of the pulsing nature, as compared to a single long-duration pulse. This loss is the basic tradeoff of allowing the HF beam to heat multiple locations simultaneously, but if the HF-induced heating is extremely quick, only a small fraction of the time is required to maintain heating anyway.

[46] Previous studies at the Tromsø facility [*Barr and Stubbe*, 1991; *Barr et al.*, 1999], using a similar exponential model, have concluded that the ERP levels there are not sufficiently high to allow beam painting to work as proposed. Although the HAARP facility has a higher ERP at

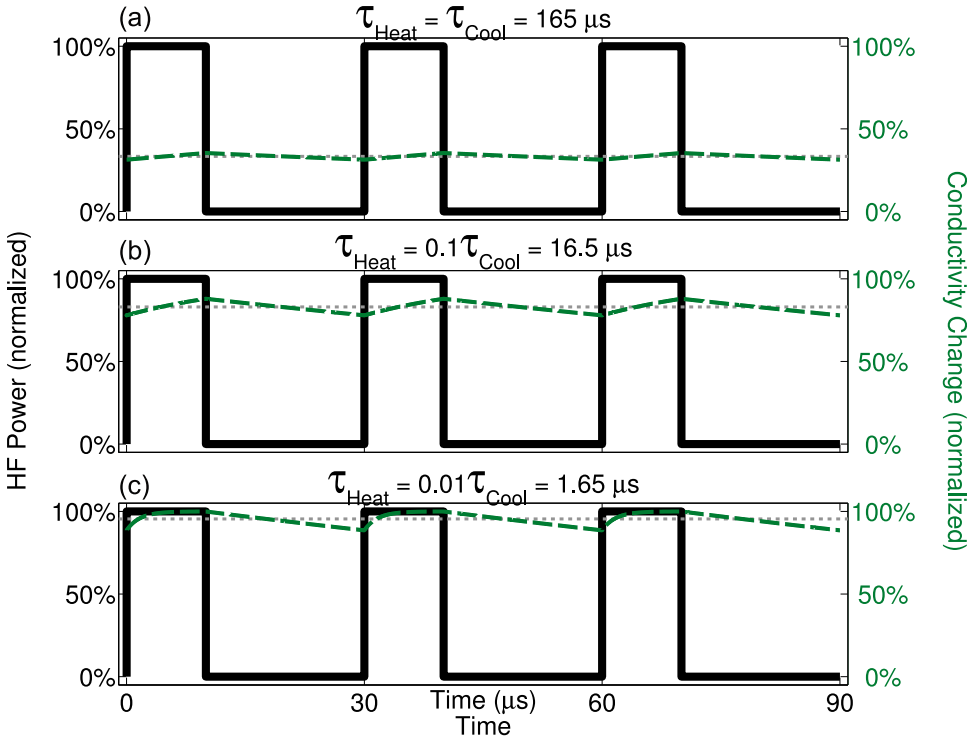

Figure 13. Schematic showing the effect of heat-cool disparity for HF pulsing at 33% pulse duty cycle and 3.33 kHz frequency. The conductivity changes for both heating and cooling are assumed to follow exponential functions with differing decay times. The cooling time constant is 165 μs. The heating time constants are (a) 165 μs, (b) 16.5 μs, and (c) 1.65 μs. The conductivity changes are shown in green; the average level is shown with a dashed gray line.

3.25 MHz (575 MW) compared to Tromsø (300 MW), it is not certain that this ERP level is high enough, either.

[47] To approach this issue theoretically, we utilize the fact that all three terms of equation (1) are proportional to the electron density for the atmospheric densities present in the *D* region. Thus the electron densities can be removed from equation (1), making it dependent only on the neutral atmospheric densities and the input HF power density at a given altitude. The heating and cooling time constants at a given altitude are independent of electron density in the ionosphere but are only affected by the HF power input (and the neutral atmospheric density), although in a stratified ionosphere, the electron densities below some altitude affects the HF power reaching that altitude. We can therefore simulate the dynamics of heating, cooling, and conductivity modulation, as a function strictly of HF power density and altitude, i.e., a zero-dimensional version of the theoretical model discussed earlier.

[48] We repeat the simulation for a series of HF power densities between 1 μW/m and 100 mW/m and a series of rapid (50 kHz cycle) ON-OFF fluctuations with pulse duty cycle varying between 2% and 98%. In following this procedure we account for the complete dynamics of the electron heating and recovery rate, and nonlinear conversion to conductivity changes, rather than assuming an exponential behavior to the conductivity. We once again focus on the Hall conductivity, due to its dominance in generating the long-distance radiation from HAARP. Utilization of the single-altitude model also allows us to remove ionospheric variability and provide a more generalized solution, and consider only the variation across altitudes, and HF power densities, without the complications of self absorption.

[49] Figure 14 shows the average conductivity change induced by pulsed HF heating. Figure 14a schematically shows some examples of the HF power modulation function applied, with varying pulse duty cycle. Figures 14b–14d show the average Hall conductivity change in steady state, at altitudes of 70 km and 90 km and for both 3.25 MHz and 9.50 MHz. The conductivity modulation is normalized to the maximum possible Hall modulation depth. At the 100% pulse duty cycle level, the average conductivity change is 100% of the maximum, whereas at 0%, no heating occurs so the conductivity change is also zero. Everywhere else, the value of the colorbar essentially illustrates a loss of conductivity modulation as a result of the finite ERP. The higher the value of the power density, the lower the pulse duty cycle that can be sustained before this loss of conductivity is significant, since higher power densities heat the electrons to the maximum temperature increasingly fast. Since the line paint involves cycling the HF beam between three locations, the pulse duty cycle is 33%, as indicated with the upper dashed line in Figures 14a and 14b. The grid paint involves alternating the HF beam between nine locations, corresponding to an 11% pulse duty cycle. The vertical dashed line shows the maximum ERP achievable with HAARP (i.e., assuming that no HF power is absorbed by the ionosphere on the way to that altitude). This maximum level is likely close to the actual ERP for 70 km altitude, since

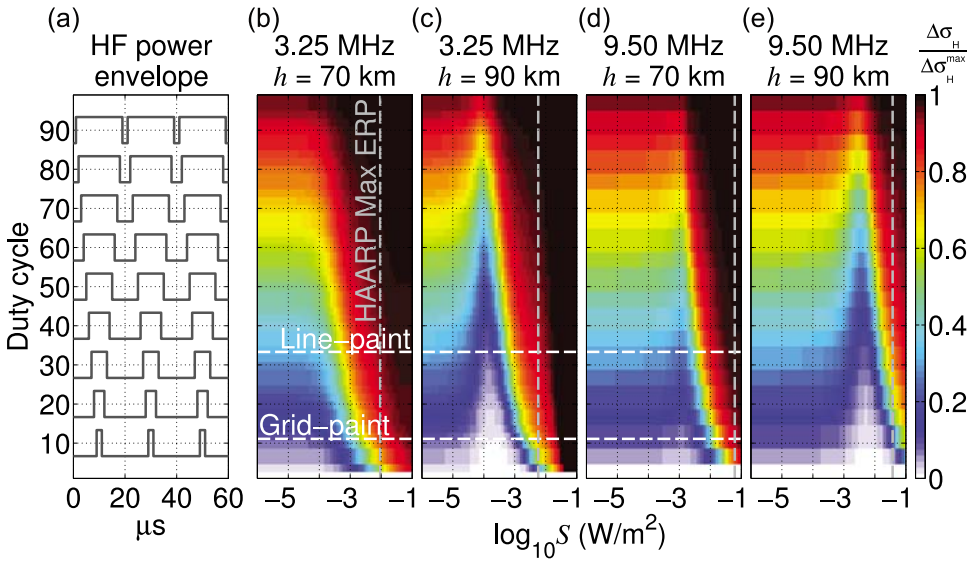

Figure 14. Loss of efficiency as a result of conductivity falls during the HF pulsing showing (a) HF power envelope at 50 kHz for a variety of pulse duty cycles and the conductivity loss (normalized to the maximum possible) for each combination of pulse duty cycle (vertical axis) and HF power density (horizontal axis) at (b) 70 km and (c) 90 km altitudes and for HF heating at (d) 3.25 MHz and (e) 9.50 MHz.

ionospheric absorption below 70 km (particularly at nighttime) is not too high, but at 90 km, the actual ERP levels reaching this altitude are likely much lower than the maximum by perhaps an order of magnitude or more, owing the significant ionospheric HF absorption between 70 and 90 km, especially during daytime.

[50] For the 575 MW ERP of HAARP at 3.25 MHz, the power density at 70 km altitude is ~9.3 mW/m^2 for free space conditions. In addition, since the ionospheric absorption below 70 km is small, even for a daytime ionosphere, the actual power density at 70 km is likely close to this value. For the line paint, the loss at the 9.3 mW power level is ~14%, while for the grid paint, it is ~5%. At 90 km altitude, a significant portion of the HF power density has been absorbed. Assuming a remaining power density of 1 mW/m^2, the conductivity loss is ~24% for the line paint (33% pulse duty cycle), and 73% for the grid paint. This conductivity loss may account for part of the fact that beam painting is apparently no more effective than amplitude modulation at longer distances from HAARP in the observations of *Cohen et al.* [2010b].

[51] At 90 km, a minimum in the efficiency is observed, at a power density of ~10^{-4} W/m^2 at 3.25 MHz, and ~$10^{-2.5}$ W/m^2 at 9.5 MHz. This effect is probably related to the so-called "translucence" effect, discussed by *Belova et al.* [1995], where the HF absorption coefficient may increase or decrease as a function of HF power density.

[52] Although the beam painting technique relies on a high ERP, it seems that even the newly upgraded HAARP facility does not always have a sufficiently high ERP (at 3.25 MHz) to completely sustain high conductivity during the beam painting technique, especially at higher altitudes and in the case of higher HF frequencies. Variations in the ionospheric electron density may impact this, since high HF power densities are needed at high altitudes in order to sustain these high conductivities, which is better achieved when the ionosphere is lightly ionized, such as in quiet nighttime conditions.

7. Conclusion

[53] The new capabilities of the HAARP array include the ability to rapidly (100-kHz rates) steer a very intense beam of HF radiation to the ionosphere. In recent experiments, this new capability has been utilized for generation of ELF and VLF radio waves via continuous or modulated HF heating. The experimental measurements provide a good picture of the properties of the generation for various modulation techniques.

[54] Our focus here is the first application of a complete end-to-end model of HF heating to ELF/VLF amplitudes for the purpose of characterizing and predicting the radiation pattern from modulated steered HF heating to as far as 1000 km from the source. We utilize this model to directly compare to observations presented by *Cohen et al.* [2010b] of beam painting and geometric modulation as compared to amplitude modulation. Results are shown to be fairly consistent between experiment and modeling.

[55] More importantly, application of this model has allowed us to describe features that cannot be measured without an unreasonable number of receiver locations. It has also allowed us to apply simpler versions of a theoretical model to isolate specific physical phenomena that impact our observations, thereby quantifying their effect. We have described the effectiveness of HAARP at maintaining conductivity changes with pulsed (or rapidly repetitive) HF heating, a feat deemed not possible with earlier HF arrays. We have applied a simpler free-space model to demonstrate the role of an ELF/VLF phased array in the geometric modulation schemes, as a result of multiple beam locations whose order is controllable, in agreement with postulates set forth by *Cohen et al.* [2008b]. Future applications of this

model may shed light on other properties of ELF/VLF wave generation with HF heating, such as magnetospheric injection.

[56] **Acknowledgments.** We acknowledge support from the Office of Naval Research (ONR), Air Force Research Laboratory, and Defense Advanced Research Programs Agency, via ONR grants N00014-09-1 and N00014-05-1-0854 to Stanford. We thank Mike McCarrick for providing the detailed HAARP HF radiation patterns.

[57] Robert Lysak thanks Tony Ferraro and Michael Rietveld for their assistance in evaluating this paper.

References

Barr, R., and P. Stubbe (1984), ELF and VLF radiation from the 'polar electrojet antenna', *Radio Sci.*, *19*(4), 1111–1122.

Barr, R., and P. Stubbe (1991), On the ELF generation efficiency of the Tromsø "super heater" facility, *Geophys. Res. Lett.*, *18*(11), 1971–1974.

Barr, R., M. T. Rietveld, P. Stubbe, and H. Kopka (1987), Ionospheric heater beam scanning: A mobile source of ELF/VLF radiation, *Radio Sci.*, *22*(6), 1076–1083.

Barr, R., M. T. Rietveld, P. Stubbe, and H. Kopka (1988), Ionospheric heater beam scanning: A realistic model of this mobile source of ELF/VLF radiation, *Radio Sci.*, *23*(3), 379–388.

Barr, R., P. Stubbe, and M. T. Rietveld (1999), ELF wave generation in the ionosphere using pulse modulated HF heating: Initial tests of a technique for increasing ELF wave generation effciency, *Ann. Geophys.*, *17*, 759–769.

Barr, R., D. Llanwyn Jones, and C. J. Rodger (2000), ELF and VLF radio waves, *J. Atmos. Sol. Terr. Phys.*, *62*, 1689–1718.

Belova, E. G., A. B. Pashin, and W. B. Lyatski (1995), Passage of a powerful HF radio wave through the lower ionosphere as a function of initial electron density profiles, *J. Atmos. Terr. Phys.*, *57*(3), 265–272.

Borisov, N., A. Gurevich, and K. Papadopoulos (1996), Direct Cerenkov excitation of waveguide modes by a mobile ionospheric heater, *Radio Sci.*, *31*(4), 859–867.

Budden, K. G. (1985), *The Propagation of Radio Waves: The Theory of Radio Waves of Low Power in the Ionosphere and Magnetosphere*, Cambridge Univ. Press, New York.

Carroll, K. J., and A. J. Ferraro (1990), Computer simulation of ELF injection in the Earth-ionosphere waveguide, *Radio Sci.*, *25*(6), 1363–1367.

Cohen, M. B., M. Gołkowski, and U. S. Inan (2008a), Orientation of the HAARP ELF ionospheric dipole and the auroral electrojet, *Geophys. Res. Lett.*, *35*, L02806, doi:10.1029/2007GL032424.

Cohen, M. B., U. S. Inan, and M. Gołkowski (2008b), Geometric modulation: A more effective method of steerable ELF/VLF wave generation with continuous HF heating of the lower ionosphere, *Geophys. Res. Lett.*, *35*, L12101, doi:10.1029/2008GL034061.

Cohen, M. B., U. S. Inan, and M. Gołkowski (2009), Reply to Comment by R. C. Moore and M. T. Rietveld on "Geometric modulation: A more effective method of steerable ELF/VLF wave generation with continuous HF heating of the lower ionosphere", *Geophys. Res. Lett.*, *36*, L04102, doi:10.1029/2008GL036519.

Cohen, M. B., U. S. Inan, and E. P. Paschal (2010a), Sensitive broadband ELF/VLF radio reception with the AWESOME instrument, *IEEE Trans. Geosci. Remote Sens.*, *48*(1), 3–17, doi:10.1109/TGRS.2009.2028334.

Cohen, M. B., U. S. Inan, M. Gołkowski, and M. J. McCarrick (2010b), ELF/VLF wave generation via ionospheric HF heating: Experimental comparison of amplitude modulation, beam painting, and geometric modulation, *J. Geophys. Res.*, *115*, A02302, doi:10.1029/2009JA014410.

Davies, K. (1990), *Ionospheric Radio*, Inst. of Electrical Engineers, London.

Getmantsev, C. G., N. A. Zuikov, D. S. Kotik, N. A. Mironenko, V. O. Mityakov, Y. A. Rapoport, V. Y. Sazanov, V. Y. Trakhtengerts, and V. Y. Eidman (1974), Combination frequencies in the interaction between high-power short-wave radiation and ionsopheric plasma, *J. Exp. Theor. Phys.*, *20*, 101–102.

Gołkowski, M., U. S. Inan, A. R. Gibby, and M. B. Cohen (2008), Magnetospheric amplification and emission triggering by ELF/VLF waves injected by the 3.6 MW HAARP ionospheric heater, *J. Geophys. Res.*, *113*, A10201, doi:10.1029/2008JA013157.

James, H. (1985), The ELF spectrum of artificially modulated D/E-region conductivity, *J. Atmos. Terr. Phys.*, *47*(11), 1129–1142.

Lehtinen, N. G., and U. S. Inan (2008), Radiation of ELF/VLF waves by harmonically varying currents into a stratified ionosphere with application to radiation by a modulated electrojet, *J. Geophys. Res.*, *113*, A06301, doi:10.1029/2007JA012911.

Lehtinen, N. G., and U. S. Inan (2009), Full-wave modeling of transionospheric propagation of VLF waves, *Geophys. Res. Lett.*, *36*, L03104, doi:10.1029/2008GL036535.

McCarrick, M. J., D. D. Sentman, A. Y. Wong, R. F. Wuerker, and B. Chouinard (1990), Excitation of ELF waves in the schumann resonance range by modulated HF heating of the polar electrojet, *Radio Sci.*, *25*(6), 1291–1298.

McNeil, J. D., and V. F. Labson (1991), Geological mapping using VLF radio field, in *Electromagnetic Methods in Applied Geophysics*, edited by M. Nabighian, chap. 7, pp. 521–640, Soc. of Explor. Geophys., Tulsa, Okla.

Moore, R. C. (2007), ELF/VLF wave generation by modulated HF heating of the auroral electrojet, Ph.D. thesis, Stanford Univ., Stanford, Calif.

Moore, R. C., and M. T. Rietveld (2009), Comment on "Geometric modulation: A more effective method of steerable ELF/VLF wave generation with continuous hf heating of the lower ionosphere" by M. B. Cohen, U. S. Inan, and M. A. Golkowski, *Geophys. Res. Lett.*, *36*, L04101, doi:10.1029/2008GL036002.

Moore, R. C., U. S. Inan, T. F. Bell, and E. J. Kennedy (2007), ELF waves generated by modulated HF heating of the auroral electrojet and observed at a ground distance of ~4400 km, *J. Geophys. Res.*, *112*, A05309, doi:10.1029/2006JA012063.

Papadopoulos, K., A. S. Sharma, and C. L. Chang (1989), On the efficient operation of a plasma ELF antenna driven by modulation of ionospheric currents, *Comments Plasma Phys. Controlled Fusion*, *13*(1), 1–17.

Papadopoulos, K., C. Chang, P. Vitello, and A. Drobot (1990), On the efficiency of ionospheric ELF generation, *Radio Sci.*, *25*, 1131–1320.

Payne, J. A. (2007), Spatial structure of very low frequency modulated ionospheric currents, Ph.D. thesis, Stanford Univ., Stanford, Calif.

Payne, J. A., U. S. Inan, F. R. Foust, T. W. Chevalier, and T. F. Bell (2007), HF modulated ionospheric currents, *Geophys. Res. Lett.*, *34*, L23101, doi:10.1029/2007GL031724.

Piddyachiy, D., U. S. Inan, and T. F. Bell (2008), DEMETER observations of an intense upgoing column of ELF/VLF radiation excited by the HAARP HF, *J. Geophys. Res.*, *113*, A10308, doi:10.1029/2008JA013208.

Rietveld, M. T., H. Kopka, and P. Stubbe (1986), D-region characteristics deduced from pulsed ionospheric heating under auroral elecrojet conditions, *J. Atmos. Terr. Phys.*, *48*(4), 311–326.

Stubbe, P., H. Kopka, and R. L. Dowden (1981), Generation of ELF and VLF waves by polar electrojet modulation: Experimental results, *J. Geophys. Res.*, *86*(A11), 9073–9078.

Tomko, A. A. (1981), Nonlinear phenomena arising from radio wave heating of the lower ionosphere, Ph.D. thesis, Penn. State Univ., University Park, Pa.

Wait, J. R., and K. P. Spies (1964), Characteristics of the Earth-ionosphere waveguide for VLF waves, *Tech. Rep. 300*, Natl. Bur. of Stand., Boulder, Colo.

Watt, A. D. (1967), *VLF Radio Engineering*, Pergamon, New York.

Werner, D. H., A. M. Albert, and A. J. Ferraro (1990), Implementation of an ELF array of ionospheric dipoles using the High-power Auroral Simulation facility, *Radio Sci.*, *25*(6), 1397–1406.

M. B. Cohen, U. S. Inan, and N. G. Lehtinen, STAR Laboratory, EE Department, 350 Serra Mall, Room 356, Stanford, CA 94305, USA. (mcohen@stanford.edu)

M. Gołkowski, Department of Electrical Engineering, University of Colorado at Denver, North Classroom 2204E, Denver, CO 80217, USA.